BSC

Model Administrative Change Notice

Complete only applicable items.

DOC.20051130.0002

1. Document Number:	ANL-EBS-MD-000027	2. Revision:	03	3. ACN:	02
4. Title:	Drift Degradation Analysis				
5. No. of Pages Attached	20				

6. Approvals:

Preparer:	Ming Lin Print name and sign	11/28/05 Date
Checker:	Junghun Leem Print name and sign	11/28/05 Date
QER:	Darrell Svalstad Print name and sign	11/28/05 Date
Independent Technical Reviewer:	Jean Younker Print name and sign	11-28-05 Date
Responsible Manager:	Richard Quittmeyer Print name and sign	11-28-2005 Date

7. Affected Pages	8. Description of Change:
viii	Self-identified correction in the Executive Summary, page viii, last paragraph, fourth and fifth sentences, "Static fatigue of hard rocks typically is associated with stress levels on the order of 80 percent or greater of the uniaxial compressive strength. This means that fatigue failure would presumably initiate along asperities on fracture surfaces, reducing their effective friction angle." are modified to read, "Fatigue failure would presumably initiate along asperities on fracture surfaces, reducing their effective friction angle."
xv	To address CR 5896, the following items are added to the Table of Contents, page xv, 6.4.2.2.3 Sensitivity of Mechanical Properties to Rockfall Predictions ..... 6-177 6.4.2.2.4 Estimation of Drift Profile for Feeds to the Abstraction of Drift Seepage ..... 6-180 6.4.2.3 Thermal Consideration in Lithophysal Units ..... 6-180 6.4.2.3.1 Thermal Loading ..... 6-180 6.4.2.3.2 Combined Seismic and Thermal Effect in Lithophysal Units ..... 6-182 6.4.2.4 Time-Dependent Consideration in Lithophysal Units ..... 6-189 6.4.2.4.1 Empirical Observations of Degradation and Collapse of Excavations ..... 6-190 6.4.2.4.2 Mechanics-Based Approach to Analysis of Time-Dependent Degradation of Repository Excavations ..... 6-197 6.4.2.4.3 Summary of Time-Dependent Consideration ..... 6-213 6.4.2.5 Quasi-Static Drip Shield Loading from Rockfall ..... 6-216 6.4.2.5.1 Introduction ..... 6-216 6.4.2.5.2 Bulking of the Rubble ..... 6-217 6.4.2.5.3 Estimation of Collapse Dimensions and Drift Profile ..... 6-218 6.4.3 Investigation of Potential Key Blocks in Lithophysal Units ..... 6-233 6.5 UNCERTAINTIES AND LIMITATIONS ..... 6-235 6.6 DRIFT DEGRADATION FEPS ..... 6-239 6.7 DOCUMENTATION OF ALTERNATIVE CONCEPTUAL MODELS ..... 6-242 6.8 RESOLUTION OF KEY TECHNICAL ISSUES 6-243

1. Document Number:	ANL-EBS-MD-000027	**2. Revision**:	03	**3. ACN**:	02
4. Title:	Drift Degradation Analysis				

4-12	Self-identified correction on page 4-12, Section 4.1.5, first paragraph, first and third sentences, "Seismic ground motion time history data were provided for the following hazard levels: 5×10-4 per year, 1×10^{-4} per year, 1×10^{-6} per year, and 1×10^{-7} per year. DTNs for each of these ground motion levels are listed in Table 4-1. The ground motion data for the postclosure ground motion levels (i.e., 1×10^{-6} and 1×10^{-7}) each include 15 sets (three components) of time histories at the repository horizon." are modified to read, "Seismic ground motion time history data were provided for the following hazard levels: 5×10^{-4} per year, 1×10^{-4} per year, **1×10^{-5} per year,** 1×10^{-6} per year, and 1×10^{-7} per year. DTNs for each of these ground motion levels are listed in Table 4-1. The ground motion data for the postclosure ground motion levels (i.e., **1×10^{-5},** 1×10^{-6} and 1×10^{-7}) each include 15 sets (three components) of time histories at the repository horizon."
4-12	Self-identified correction of the DIRS report and reference call out on page 4-12, Section 4.1.5, first paragraph, last sentence, "Conditioning on expected peak particle velocity alone was considered desirable as damage to underground structures is most strongly correlated with this point measurement, recognizing that underground (at-depth) spectral shapes are generally not identical to surficial or outcrop spectral shapes due to the effects of down going wave fields (BSC 2004 [DIRS 170027], Section 6.3.2)." is modified to read, "Conditioning on expected peak particle velocity alone was considered desirable as damage to underground structures is most strongly correlated with this point measurement, recognizing that underground (at-depth) spectral shapes are generally not identical to surficial or outcrop spectral shapes due to the effects of down going wave fields (BSC 2004 [DIRS 170027], Section 6.3.**1.5**)."
6-5	Self-identified correction on page 6-5, first paragraph. "The central block of Yucca Mountain is bounded by the Yucca Wash to the north, by the Solitario Canyon fault to the west, and the Bow Ridge fault to the east (Figure 6-2)." is modified to read, "The central block of Yucca Mountain is bounded by the Solitario Canyon fault to the west, and the Bow Ridge fault to the east (Figure 6-2)."
6-6	Self-identified correction on page 6-6, Figure 6-2 contained text that was illegible. The figure has been replaced to clarify the illegible text. Note: The new figure is based on the same source as the replaced figure and has no impact on the results of the Drift Degradation Analysis report.
6-11	Self-identified correction on page 6-11, text within Figure 6-4 was changed to correct a typographical error. The abbreviation for Middle Nonlithophysal was "Tptpll" and corrected to "Tptpmn". Note: There were no other changes to the figure and the change has no impact on the results of the Drift Degradation Analysis report.

1. Document Number:	ANL-EBS-MD-000027	2. Revision:	03	3. ACN:	02
4. Title:	Drift Degradation Analysis				

6-48	Self-identified correction on page 6-48, second item in sub-list at the top of the page, "−Heat Capacity: 811 J/kg-K (= 954 J/kg-K – one standard deviation [143 J/kg-K])." is modified to read, "− **Specific** Heat: 811 J/kg-K (= 954 J/kg-K – one standard deviation [143 J/kg-K])."
6-48	Self-identified correction on page 6-48, first paragraph, third, fourth and fifth sentences, "The heat capacity data used in the thermal analyses were preliminary and have been superseded by *Heat Capacity and Thermal Expansion Coefficients Analysis Report* (BSC 2003 [DIRS 164670], Table 6-5) and DTN: SN0307T0510902.003 [DIRS 164196] (see Appendix E, Table E-16). In this document, heat capacity values for the range of T ≤ 95°C only were utilized for the thermal calculations using the LDTH sub-model (Table E-16). Because consideration of latent heat effects above the boiling point is built into the NUFT code, the high heat capacity value at the temperature range of 95 to 114°C (Table E-16) were not used in the thermal calculations in this document." is modified to read, "The **specific** heat data **(also known as heat capacity)** used in the thermal analyses were preliminary and have been superseded by *Heat Capacity and Thermal Expansion Coefficients Analysis Report* (BSC 2003 [DIRS 164670], Table 6-5) and DTN: SN0307T0510902.003 [DIRS 164196] (see Appendix E, Table E-**19**). In this document, **specific** heat values for the range of T ≤ 95°C only were utilized for the thermal calculations using the LDTH sub-model (Table E-**19**). Because consideration of latent heat effects above the boiling point is built into the NUFT code, the high **specific** heat value at the temperature range of 95 to 114°C (Table E-**19**) were not used in the thermal calculations in this document."
6-64	Self-identified correction of a typographical error on page 6-64. Table 6-5, far right column, third cell from the bottom, the value in the cell is changed from "30.0" to "**30.70**"
6-64	Self-identified correction to the second sentence of the NOTE below Table 6-5. "Seismic induced stress (column six) is calculated based on elastic wave equations (Itasca Consulting Group 2002 [DIRS 160331], Manuals/3DEC/Optional Features/Section 2: Dynamic Analysis, Section 2.5)." is modified to read, "Seismic induced stress (column six) is calculated based on elastic wave equations (Itasca Consulting Group 2002 [DIRS 160331], Manuals/3DEC/Optional Features/Section 2: Dynamic Analysis, Section 2.5) **using the Young's modulus and Poisson's ratio values from Table 6-3 and the mean density value from Table E-2**."

1. Document Number:	ANL-EBS-MD-000027	2. Revision:	03	3. ACN:	02
4. Title:	Drift Degradation Analysis				

6-236	Self-identified correction on page 6-236, last paragraph, third sentence, "Finally, randomness in the spectral content and duration of time histories that produce the same peak ground motion is accommodated in the drift degradation analyses through the use of 15 sets of time histories for each of the two postclosure hazard levels considered." is modified to read, "**Finally, randomness in the spectral content and duration of time histories that produce the same peak ground motion is accommodated in the drift degradation analyses through the use of 15 sets of time histories for each of the postclosure hazard levels considered."**
7-38	This change is associated with CR-5600. End of 2nd paragraph on page 7-38, add to read: **"The tensile strength test data for the large core lithophysal sample is not available. The relationship of the uniaxial compressive strength and uniaxial tensile strength is used for the selection of the uniaxial tensile strength. Jaeger and Cook (1979, [DIRS 106219], p. 190) stated that the value of the uniaxial compressive strength is eight or twelve times that of the uniaxial tensile strength. The tensile strength of 0.8 MPa (approximately one twelfth of the 10 MPa uniaxial compressive strength) was therefore selected as the target value for the tensile test numerical experiment. This is adequate for the intended use in the calibration exercise."**
7-39	This change is associated with CR-5600. Figure 7-21 "Numerical Experiment, Category 1: Failure Envelope", on page 7-39 has been replaced to correct typographical error on the legend of the figure. Note: This change to the figure has no impact on the results of the Drift Degradation Analysis report.
9-22	Reference information is added to Section 9.4. This is a self-identified correction. "MO0014RIB00035.001. Rock Thermal Expansion. Submittal date: 04/07/2000. 153848"
C-9	Self-identified correction on page C-9, last paragraph, first sentence, "The heat capacity data used in the thermal property calculation (Table C-4) were preliminary data superseded by DTN: SN0307T0510902.003 [DIRS 164196] (Table E-19)." is modified to read, "The **specific** heat data used in the thermal property calculation (Table C-4) were preliminary data superseded by DTN: SN0307T0510902.003 [DIRS 164196] (Table E-19)."
E-28	A new column is added to far right of Table E-10. This edit is self-identified. Add a heading titled "**Lithophysal Porosity Ranges for Rock Mass Categories[b] (%)**" and these values in the five rows underneath the heading title; **">25**"; "**20 –25**"; "**15 – 20**", "**10 – 15**"; and "**<10**".

1. Document Number:	ANL-EBS-MD-000027	2. Revision:	03	3. ACN:	02
4. Title:	Drift Degradation Analysis				

E-28	Table E-10 footnote “b”, was changed in ANL-EBS-MD-000027 REV 03 ACN 01. This correction was associated with TBV-5811. “BSC 2004 [DIRS 168970], Table 6.6-1.” was changed to, **“**BSC 2004 [DIRS **172334**], Table **6.4-1.”**
E-56	The NOTE below Table E-20 is edited. This change is associated with CR-5497 “Source data provided by DTN: SNL01B05059301.006 [DIRS 129168]. Thermal expansion data are for saturated rock. The calculation of mean data is documented in Brodsky et al. (1997 [DIRS 100653], Table 4-4).” is modified to read, “Source data provided by DTN: SNL01B05059301.006 [DIRS 129168]. Thermal expansion data are for saturated rock. **The use of saturated data (as opposed to dry data) results in higher thermal stresses and is therefore more conservative for use in drift degradation analyses.** The calculation of mean data is documented in Brodsky et al. (1997 [DIRS 100653], Table 4-4). **The standard deviation data presented in Brodsky et al. (1997 [DIRS 100653], Table 4-4) are not used in this report since they are relatively small and do not significantly impact the calculation of thermal stress in this report. Additional thermal expansion data have been provided by DTN: MO0004RIB00035.001 [DIRS 153848]. The mean values for the additional data are similar to the data in this table, and the inclusion of the additional thermal expansion data would not significantly impact the results from this analysis. Therefore, the additional thermal expansion data have not been included in this report**.”
Q-8	Seven instances of the term “heat capacity” are changed to read “**specific heat**” (including the appendix section title, the second and sixth sentences of the first paragraph, twice in the first sentence of the second paragraph, and the first and third sentences of the third paragraph. These corrections are self-identified.
Q-8	In the first paragraph, sixth sentence, a hyphen is inserted between the words “equation” and “defined” so that the words read “**equation-defined**.” This correction is self-identified.

The geologic structure and rock strength defines the failure mode in the Tptpmn. The failure mode in the Tptpmn is due to gravity drop of rock blocks resulting from stress-induced yield in either the intact rock or the joint surfaces. The analysis of the failure mechanism is complicated somewhat by the fact that the jointing in the Tptpmn is of relatively short continuous trace length and is discontinuous in nature, thus forming fewer kinematically removable blocks. This type of jointing results in an inherently stronger rock mass as opposed to typical "blocky" rock masses where the block structure is well defined by multiple, continuous joint sets.

The Tptpll is characterized by about 10 to 30 percent lithophysal cavities by volume. This unit has abundant small-scale fractures between lithophysae that result in the relatively weaker nature of the material. Rock mass failure in the Tptpll is controlled by the transient ground motion induced stress concentrations that occur around the excavation. The mode of failure is primarily via tension from rarefaction of vertically traveling compression waves.

Seismic Ground Motion–Site-specific ground motions have been determined based on results from a probabilistic seismic hazard analysis. For a suite of ground motion measures, the probabilistic seismic hazard analysis determined the annual probability that various levels of ground motion would be exceeded. For an annual probability of exceedance of interest, a site response model modifies the ground motion from the probabilistic seismic hazard analysis by taking into account the effect of local site materials. Peak ground velocity determined from the site response model is used to develop seismic time histories (typically fifteen three-component sets) for postclosure rockfall analysis. The time histories are developed such that observed randomness among time histories, for a given peak ground velocity, is maintained. The time histories thus appropriately reflect variability in ground motion estimation for Yucca Mountain.

Thermal Stress–Once the waste packages are placed within the emplacement drifts, heat will be released as a part of the process of the radioactive materials in the waste packages becoming less radioactive over time. This heat will transfer to the rock mass and thermally induced stresses will be generated by thermal expansion of the rock mass. Thermal stresses at any location depend on the proximity and timing of waste emplacement, the amount of heat generated, the age of the waste, packaging and emplacement configuration, ventilation of the emplacement drifts, and the thermal-mechanical properties of the rock mass. Thermal stresses are time-dependent and are calculated over the 10,000-year regulatory period for postclosure performance.

Time-Dependent Degradation of Rock Strength–The rock mass surrounding the emplacement drifts may undergo over-stressing from thermal heating or time-dependent damage associated with static fatigue resulting from stress corrosion mechanisms. This damaged material may result in a slow unraveling (lithophysal rock) or block fallout (nonlithophysal rock). In the nonlithophysal rocks, static fatigue failure of roughness along fracture surfaces is possible and could result in gravitationally induced block failures. Fatigue failure would presumably initiate along asperities on fracture surfaces, reducing their effective friction angle. In the case of the lithophysal rocks, the compressive stress concentrations along the immediate rib springline of the emplacement drifts will be near the uniaxial compressive strength so static fatigue failure is a distinct possibility.

CONTENTS (Continued)

Page

CONTENTS (Continued)

Page

mass. Poisson's ratio for the rock mass was determined to be equal to the Poisson's ratio from intact laboratory tests based on recent field testing (see Appendix E, Table E-16).

4.1.4.3 Rock Mass Properties for the Heated Drift in the ESF

Rock mass properties for the Heated Drift are calculated using the Hoek-Brown failure criterion (Hoek et al. 2002 [DIRS 162204]) as documented in Appendix E (Section E4.2). The inputs needed include rock mass classification data using the Q system as provided in Appendix E (Table E-13). Additionally, intact unconfined compressive strength (σ_{ci}) is required input for the Hoek-Brown method (Table E-14). The calculated rock mass properties using these data are provided in Appendix E (Table E-15).

4.1.4.4 Block Strength of Nonlithophysal Rock

The strength of large-scale intact rock block material (i.e., between joints) for nonlithophysal rock is calculated based on available size-effect laboratory compression test data from Price (1986 [DIRS 106589]). The size-effect data are presented in Appendix E (Table E-17). The approach for extrapolating this data to the block scale is documented in Appendix E (Section E4.4).

4.1.5 Seismic Ground Motion Data

Seismic ground motion time history data were provided for the following hazard levels: 5×10^{-4}per year, 1×10^{-4} per year, 1×10^{-5} per year, 1×10^{-6} per year, and 1×10^{-7} per year. DTNs for each of these ground motion levels are listed in Table 4-1. The ground motion data for the postclosure ground motion levels (i.e., 1×10^{-5}, 1×10^{-6} and 1×10^{-7}) each include 15 sets (three components) of time histories at the repository horizon. The sets were developed by scaling recorded motions such that their integrated peak particle velocities match expected point repository horizon particle velocities for the hazard level under consideration. Additionally, a desirable feature of the 15 sets is a magnitude distribution reflective of the horizontal component peak particle velocity deaggregation. This ensures a reasonable and defensible distribution of spectral shapes and time history durations. Conditioning on expected peak particle velocity alone was considered desirable as damage to underground structures is most strongly correlated with this point measurement, recognizing that underground (at-depth) spectral shapes are generally not identical to surficial or outcrop spectral shapes due to the effects of down going wave fields (BSC 2004 [DIRS 170027], Section 6.3.1.5).

The ground motion data for preclosure annual exceedance probabilities (i.e., 5×10^{-4} and 1×10^{-4}) consist of a single three-component set of time histories. These sets were developed such that the response spectra of the time histories match the design response spectra for the hazard level at the repository horizon.

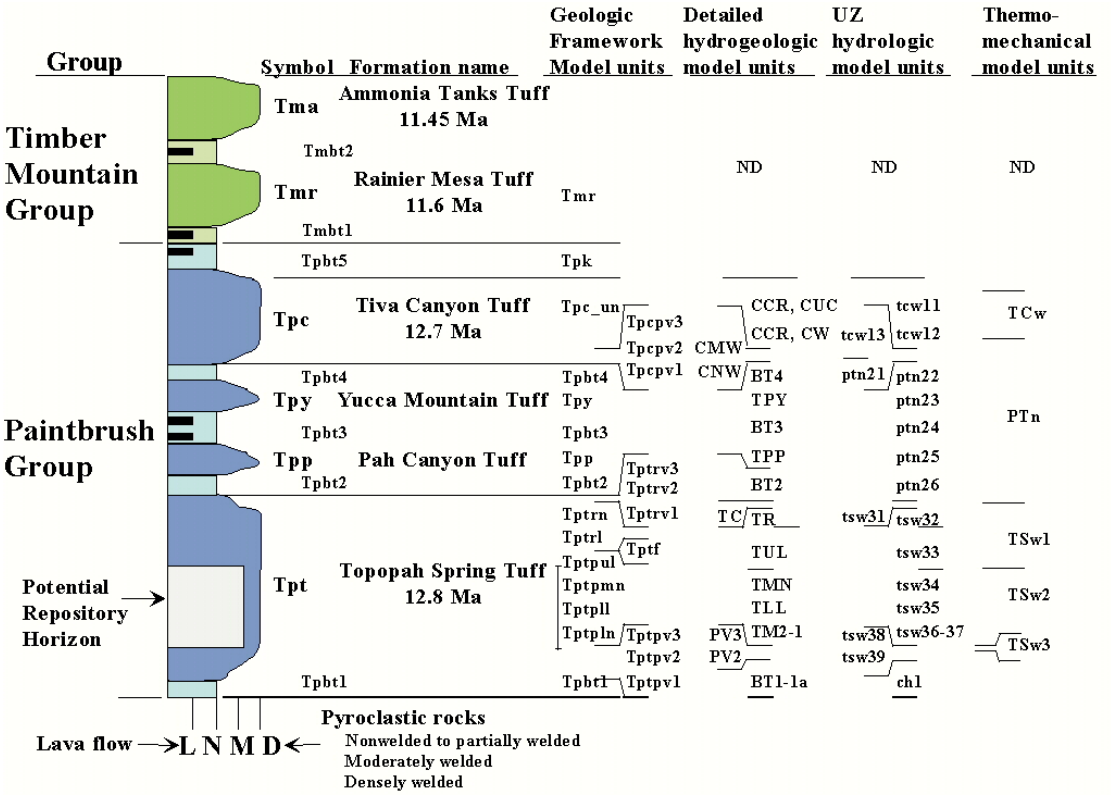

Figure 6-1. Simplified Lithostratigraphic Column of Paintbrush Group and the Rock Units that Form the Repository Host Horizon

The central block of Yucca Mountain is bounded by the Solitario Canyon fault to the west, and the Bow Ridge fault to the east (Figure 6-2). Alluvium-filled structural valleys, consisting mostly of alluvial fan deposits (fluvial and colluvial sediments) and some thin eolian deposits, lie adjacent to the Bow Ridge and Solitario Canyon faults on the east and west sides, respectively. The Yucca Mountain area is cut by steeply dipping, north–south-striking normal faults, which separate the Tertiary volcanic rocks into blocks one to four km wide (Scott 1990 [DIRS 106751]; Day et al. 1998 [DIRS 100027]). The Solitario Canyon and Ghost Dance faults dip steeply toward the west, and displacement, amount of brecciation, and number of associated splays vary considerably along their trace (Scott and Bonk 1984 [DIRS 104181]; Day et al. 1998 [DIRS 100027]). The Solitario Canyon fault has normal down-to-the-west displacement of about 260 m in the vicinity of the repository block (Mongano et al. 1999 [DIRS 149850], p. 60). The Ghost Dance fault is in the central part the repository block and is a generally north-striking normal fault zone, with down to the west displacement. The Sundance fault is located in the north-central portion of the repository block. It is a northwest-striking, east-dipping normal fault with a maximum cumulative down-to-the-northeast displacement of 6 to 11 m (Day et al. 1998 [DIRS 100027]). Numerous smaller faults and fault zones are present throughout the repository block, generally north-trending with offsets less than 5 m (Mongano et al. 1999 [DIRS 149850]).

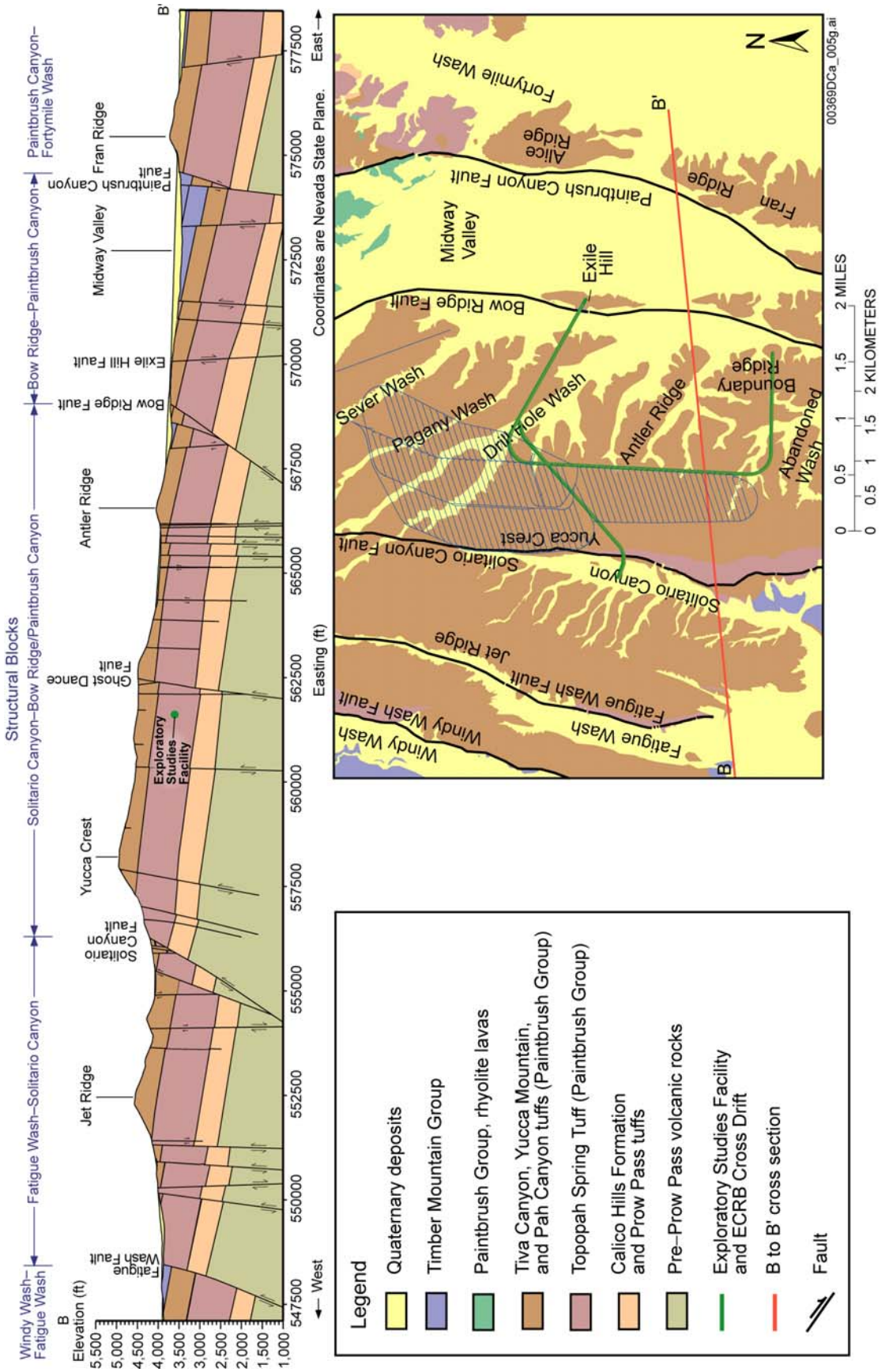

Source: Simplified from Day et al. 1998 [DIRS 100027].

Figure 6-2. Geology of the Central Block at Yucca Mountain and Location of the ESF, Including the ECRB Cross-Drift

6.1.2 Lithostratigraphy at the Repository Horizon

All of the rocks of the repository host horizon lie within the Topopah Spring Tuff—specifically within the crystal-poor member—and geochemically these rocks have a very uniform composition of rhyolite (Peterman and Cloke 2002 [DIRS 162576]). The repository host horizon includes rocks from the lower part of the upper lithophysal zone (Tptpul) of the TSw1 thermal-mechanical unit and the TSw2 thermal-mechanical unit, including the middle nonlithophysal zone (Tptpmn), the lower lithophysal zone (Tptpll), and the lower nonlithophysal zone (Tptpln) (Figure 6-1). These lithostratigraphic units are described in this section and are based on Mongano et al. (1999 [DIRS 149850]) unless otherwise indicated.

In the densely welded and crystallized rocks of the Topopah Spring Tuff, the zones and many of the subzones are identified on the basis of the abundance, size, and distribution (or lack thereof) of lithophysae, which are cavities in the rock formed during welding from the accumulation of the vapor phase. Lithophysae, spots (which are similar to the rims on lithophysae, but there is no cavity), and many fractures have similar characteristics, such as rims, borders, and possibly vapor-phase mineral coatings (Figure 6-3).

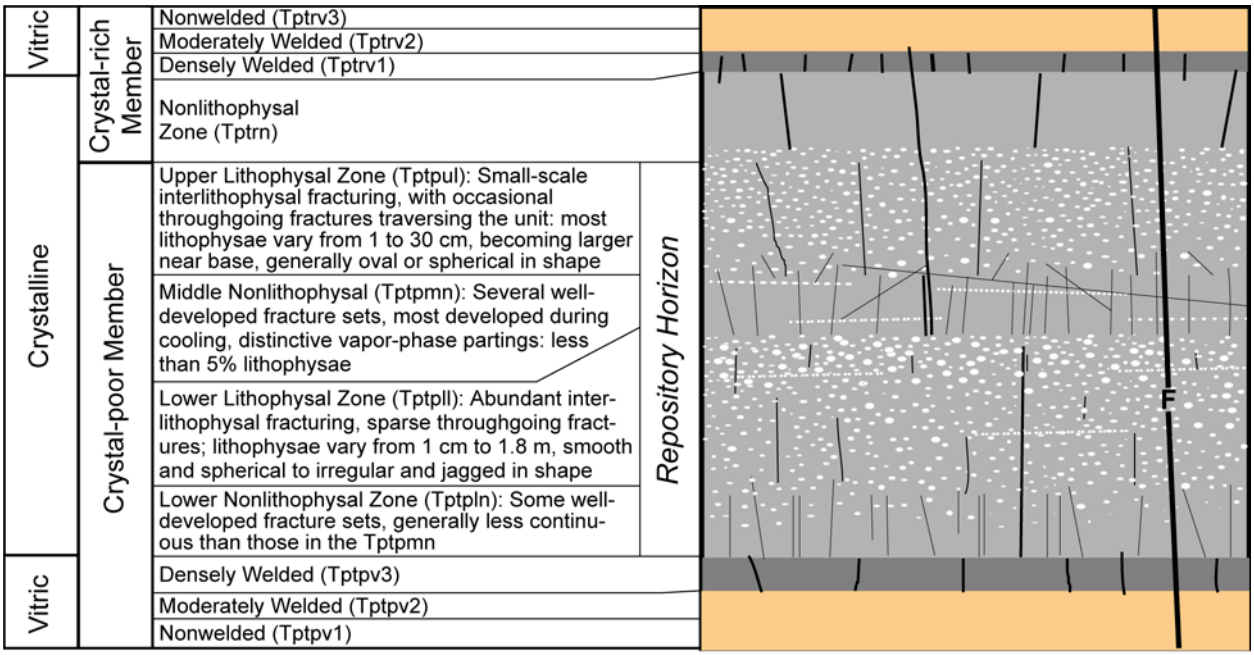

Diagrammatic Cross Section of the Topopah Spring Tuff Illustrating Relative Discontinuity Densities and Orientations: This figure indicates how fractures, faults, and lithophysae are typically distributed through the ignimbrite.

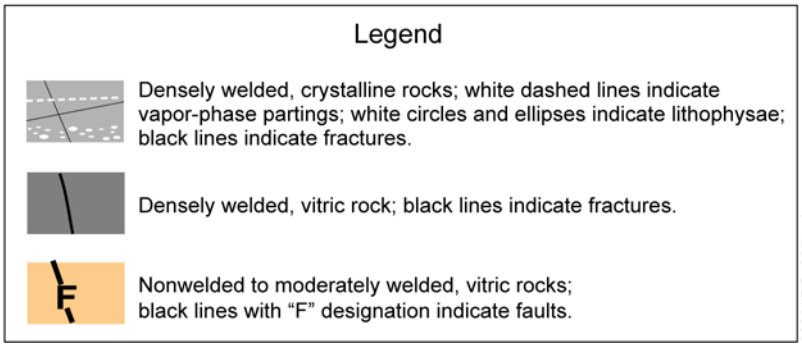

Source: Buesch et al. 1996 [DIRS 100106], Appendix 2; Mongano et al. 1999 [DIRS 149850], pp. 12 to 43.

Figure 6-4. Schematic Illustration of the Structure of the Topopah Spring Tuff

heat removal ratio. Values of thermal conductivity and specific heat one standard deviation less than the mean values were used:

- Thermal Conductivity (DTN: SN0404T0503102.011 [DIRS 169129]): 1.64 W/m-K (= 1.89 W/m-K – one standard deviation [0.25 W/m-K]) for wet conditions and 1.03 W/m-K (= 1.28 W/m-K – one standard deviation [0.25 W/m-K]) for dry conditions.

- Specific Heat: 811 J/kg-K (= 954 J/kg-K – one standard deviation [143 J/kg-K]).

- Case 3: Sensitivity calculation for heat removal ratio. 70 percent heat removal ratio was used for the preclosure ventilation (Section 5.1).

The LDTH sub-model that was used in the thermal-mechanical analysis presented in this document has been superseded by a new LDTH sub-model (DTN: LL030808623122.036 [DIRS 165790]). The new LDTH sub-model updated several input parameters including rock mass thermal property data and preclosure ventilation efficiency data. The specific heat data (also known as heat capacity) used in the thermal analyses were preliminary and have been superseded by *Heat Capacity and Thermal Expansion Coefficients Analysis Report* (BSC 2003 [DIRS 164670], Table 6-5) and DTN: SN0307T0510902.003 [DIRS 164196] (see Appendix E, Table E-19). In this document, specific heat values for the range of $T \leq 95°C$ only were utilized for the thermal calculations using the LDTH sub-model (Table E-19). Because consideration of latent heat effects above the boiling point is built into the NUFT code, the high specific heat value at the temperature range of 95 to 114°C (Table E-19) were not used in the thermal calculations in this document. The new LDTH sub-model uses a drift location-dependent and time-dependent heat removal ratio (DTN: MO0306MWDALAFV.000 [DIRS 163961]) instead of a constant heat removal ratio (Section 5.1.2) as was assumed in the rock mass temperature calculations performed in this document. This new logic considers that ventilation air will have a varying heat removal capacity as it travels from the entrance to the exit of an emplacement drift. The heat removal capacity will also vary as a function of time as both the waste package power output and rock mass temperature change (BSC 2004 [DIRS 169862]). These changes could potentially cause a significant difference in drift wall temperature during the preclosure period. Further details of the new LDTH sub-model can be found in *Multiscale Thermohydrologic Model* (BSC 2004 [DIRS 169565]).

Impact analyses were conducted regarding the new LDTH sub-model and are presented in Appendix Q (Section Q2). The impact analyses show that the use of the new LDTH sub-model primarily impacts preclosure temperature. The impact on the prediction of rock mass stress and drift degradation is insignificant.

Decay curves of the linear heat load used in the calculation cases are presented in Figure 6-24. The original linear heat decay curve (no ventilation) was obtained from *D&E/PA/C IED Subsurface Facilities* (BSC 2004 [DIRS 167369]). Ninety percent of the constant ventilation heat removal ratio (Section 5.1) was applied for Cases 1 and 2, while 70 percent of constant heat removal ratio (Section 5.1) was used in Case 3.

Table 6-5. Peak Ground Motion Parameters

Annual Hazard Level	Ground Motion Component	Peak Acceleration (g)	Peak Velocity (cm/sec)	Peak Displacement (cm)	Seismic Induced Stress Corresponding to Peak Velocity (MPa)
5×10^{-4}	H1	0.19	19.00	12.86	1.09
	H2	0.18	17.72	12.37	1.02
	V	0.22	17.73	11.34	1.68
1×10^{-4}	H1	0.39	38.38	44.44	2.20
	H2	0.37	43.78	45.30	2.51
	V	0.47	47.51	31.73	4.50
1×10^{-5} Ground Motion Set 1	H1	2.77	104.58	20.06	6.00
	H2	2.50	83.31	14.37	4.78
	V	2.63	70.88	13.00	6.71
1×10^{-6} Ground Motion Set 1	H1	7.42	244.14	16.76	14.009
	H2	6.74	195.41	26.78	11.21
	V	4.90	111.29	13.75	10.54
1×10^{-7} Ground Motion Set 1	H1	16.28	535.26	58.68	30.70
	H2	14.79	428.42	58.72	24.57
	V	13.15	298.44	36.86	28.25

Source: DTNs: MO0407TMHIS104.003 [DIRS 170599]; MO0306SDSAVDTH.000 [DIRS 164033]; MO0402AVDTM105.001 [DIRS 168890]; MO0403AVDSC106.001 [DIRS 168891]; MO0403AVTMH107.003 [DIRS 168892].

NOTES: Native data files (available as ASCII text files) containing the acceleration, velocity, and displacement time-history data can be downloaded from the source DTNs.

Seismic induced stress (column six) is calculated based on elastic wave equations (Itasca Consulting Group 2002 [DIRS 160331], Manuals/3DEC/Optional Features/Section 2: Dynamic Analysis, Section 2.5), using the Young's modulus and Poisson's ratio values from Table 6-3 and the mean density value from Table E-2.

Peak ground motion parameters for the ground motion sets are provided in Appendix X.

In running the 3DEC seismic simulation, the duration of the seismic time histories was truncated to that portion of the records displaying the majority of the energy. Initially, records were truncated to a duration bracketed by the 5 percent and 95 percent points in the energy buildup as measured by the Arias Intensity. For each three-component set of ground motions, these points were determined for each component (H1, H2, and V) and then the earliest 5 percent point and the latest 95 percent point were used to define the duration for that set of ground motions. Because preliminary analyses showed that rockfall continued in some cases beyond the 95 percent energy buildup point, additional time was added for analyses to ensure that the simulated duration covered the rockfall. Table 6-7 presents the total duration of each set of time histories and the 5 percent and 95 percent points. The sensitivity of rockfall to the duration of seismic ground motion is examined in Section 6.3.1.6.

6.3.1.2.2 Combinations of Ground Motion and Fracture Pattern

Rockfall is part of the seismic scenario calculations in support of the Total System Performance Assessment for the License Application. The analysis results provide inputs to the drip shield structural response calculation for assessment of the structural integrity of drip shields. To

ensure that the ultimate performance measure of interest (i.e., damaged surface area of the drip shield) can be tracked to the underlying uncertain inputs in a consistent fashion, a sampling

mass properties for lithophysal rock and fracture geometry in nonlithophysal rock have the greatest impact on drift degradation. The seismic ground motions, particularly those at low annual probability levels, have a large impact on stability of both nonlithophysal and lithophysal rock masses.

Rock Mass Mechanical Properties Data–Rock mass mechanical properties data for nonlithophysal rock are calculated using rock mass classification data collected from field mapping within the ESF and intact rock properties data collected from laboratory testing. The uncertainties associated with the intact rock properties data are described above. The uncertainties associated with the rock mass classification data are epistemic, and are assessed to be low because an abundance of data has been collected based on established, industry-accepted methods. There is a moderate degree of epistemic uncertainty associated with the calculation approach for assessing rock mass properties, since they are based on empirical methods and have an inherent characteristic of imprecision. This uncertainty has been accounted for by using two separate empirical calculation methods and demonstrating that the results are similar. The rock mass properties data are primarily used in the thermal-mechanical calculation to determine stresses within the model as described in Section 6.2, and are a relatively insensitive parameter to the stress calculations.

Rock mass mechanical properties data for lithophysal rock are based on large-diameter uniaxial compression test data and in situ slot test data (Appendix E, Section E4.1). The epistemic uncertainty associated with this rock mass data for lithophysal rock is assessed to be high. To account for this uncertainty in the rockfall model for lithophysal rock, five categories of rock properties were included in the model to assess the impact of the ranges in rock mass properties data. Additionally, the PFC numerical model was calibrated to reproduce the large-core laboratory mechanical properties data and its dependency on lithophysal porosity as well as the observed failure mechanisms. The model was then used to build confidence in the understanding of the bounding ranges of lithophysal rock mass properties through numerical extrapolations to examine the effect of lithophysal cavity porosity, size, shape and distribution variability as defined by field mapping. This work is described in detail in Appendix E, Section E4.1. The impact of use of the range of rock properties on drift degradation and rockfall was explored through use of sensitivity studies in Section 6.4.

Seismic Ground Motion Data–The seismic time histories used to evaluate rockfall reflect a number of variabilities, including epistemic uncertainty and randomness (aleatoric uncertainty). Epistemic uncertainties (due to incomplete knowledge) in the characterization of seismic sources and median ground motion attenuation, along with randomness in seismic ground motion, were explicitly incorporated into the probabilistic seismic hazard analysis. The mean results of that analysis form the basis for the site-specific ground motions used in this report. At annual probabilities of exceedance lower than about 1×10^{-6}, the mean hazard exceeds the 85th percentile of the hazard uncertainty distribution.

Development of site-specific ground motions incorporates additional epistemic uncertainty in the velocity and dynamic properties of site materials. Observed randomness of site materials is also addressed. Finally, randomness in the spectral content and duration of time histories that produce the same peak ground motion is accommodated in the drift degradation analyses through the use of 15 sets of time histories for each of the postclosure hazard levels considered. The

Calibration of strength micro properties involves matching macro failure envelope and post-peak behavior by adjusting strength micro-properties. Note that model plastic deformation appears to be a function of the size and shape of blocks. The failure envelope, which, in general, is a surface in the principal stress space, reduces to a line if it is considered that the failure envelope is not a function of the intermediate principal stress. Test runs have proven that the micro friction angle, which is initially equal to 35° and softens in a brittle fashion to 15°, results in the desired post-peak behavior and strength increase as a function of confinement. In order to match the observed mode of failure of non-lithophysal tuff under unconfined loading conditions (i.e., axial splitting), the micro tensile strength is assigned to be less than 50 percent of the micro cohesion. After these relations are established, the proper peak strength is matched by rescaling micro cohesion and tensile strength.

Stress-strain curves obtained from numerical experiments with different conditions of confinement (unconfined, 1-MPa confinement, and 3-MPa confinement) and loading (tension and compression) are shown in Figure 7-20. The mode of failure is also illustrated for each case by a plot of displacement vectors at the final state of the model. The model matches unconfined compressive strength of 10 MPa and Young's modulus of 1.9 GPa for Category 1 (Table E-10). Laboratory testing data on the post-peak behavior of lithophysal rock is inconclusive. However, the model exhibits qualitatively reasonable post-peak behavior. The response for low confinement is brittle (see unconfined compressive strength curve in Figure 7-20). As confinement increases the response becomes more ductile, almost perfectly plastic for 3-MPa confinements (Figure 7-20). The mode of sample failure in the case of unconfined compressive strength is axial splitting, similarly to observations from laboratory experiments. The mode of failure for confined cases becomes more of the "shear band" type. The tensile strength test data for the large core lithophysal sample is not available. The relationship of the uniaxial compressive strength and uniaxial tensile strength is used for the selection of the uniaxial tensile strength. Jaeger and Cook (1979 [DIRS 106219], p. 190) stated that the value of the uniaxial compressive strength is eight or twelve times that of the uniaxial tensile strength. The tensile strength of 0.8 MPa (approximately one twelfth of the 10 MPa uniaxial compressive strength) was therefore selected as the target value for the tensile test numerical experiment. This is adequate for the intended use in the calibration exercise.

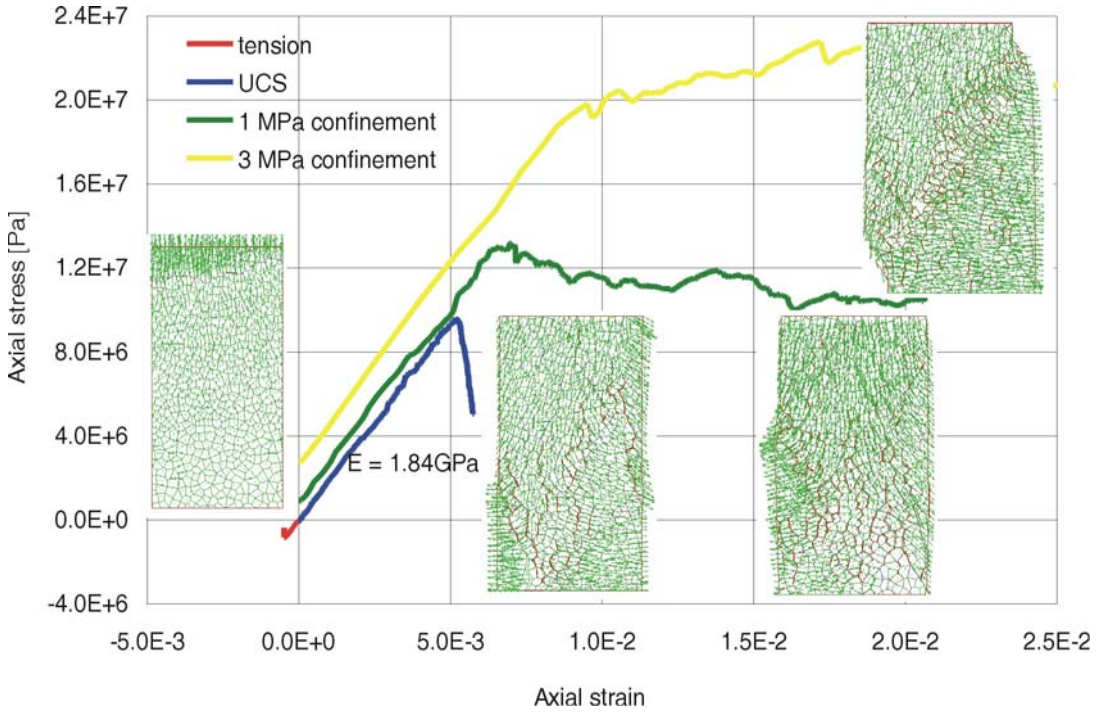

Figure 7-20. Numerical Experiment, Category 1: Stress-Strain Curves and Modes of Failure for Different Confinements and Loading Conditions

The failure envelope in the principal stress space, constructed based on numerical tests at different confinement levels, is shown in Figure 7-21. The failure envelope is curvilinear, as expected for a rock mass (similar to Hoek-Brown failure criterion). The initial friction angle (in the range of confining stress, σ_3, between 0 and 1 MPa) is 33°, but it decreases for larger confinement. The ratio between uniaxial compressive and tensile strengths is larger than 10.

The volumetric deformation of the model during the experiments is illustrated in Figure 7-22, which shows curves of volumetric strain versus axial strain. In general, these curves are bilinear. Initially, while the sample behaves elastically, its volume reduces due to the Poisson's effect. The initial slope of the curves is a function of the Poisson's ratio. Thus, the Poisson's ratio, ν, of the synthetic material can be calculated from the initial slope of the curve, s_e, according to the following formula derived from elasticity theory:

$$\nu = \frac{1 - s_e}{2 - s_e} \qquad \text{(Eq. 7-5)}$$

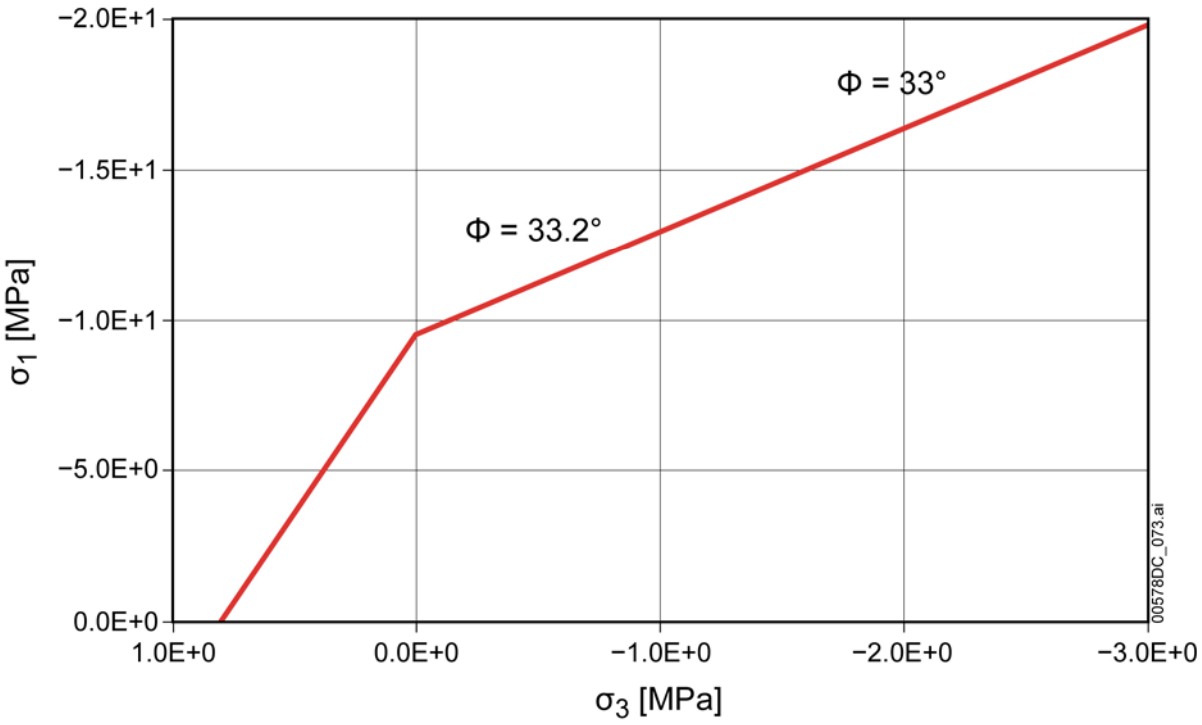

Figure 7-21. Numerical Experiment, Category 1: Failure Envelope

LADB831321AN98.002. Revised Mineralogic Summary of Yucca Mountain, Nevada. Submittal date: 05/26/1998. 109003

LADV831321AQ97.001. Mineralogic Variation in Drill Holes. Submittal date: 05/28/1997. 107142

LADV831321AQ99.001. Quantitative XRD Results for the USW SD-6 and USW WT-24 Drill Core Samples. Submittal date: 04/16/1999. 109044

LB0205REVUZPRP.001. Fracture Properties for UZ Model Layers Developed from Field Data. Submittal date: 05/14/2002. 159525

LB0208UZDSCPMI.002. Drift-Scale Calibrated Property Sets: Mean Infiltration Data Summary. Submittal date: 08/26/2002. 161243

LL030808623122.036. Input and Output Files for NUFT MSTHM Sub-Models Supporting LA Multi-Scale Analyses. Submittal date: 09/11/2003. 165790

MO0001SEPDSTPC.000. Drift Scale Test (DST) Temperature, Power, Current, and Voltage Data for June 1, 1999 through October 31, 1999. Submittal date: 01/12/2000. 153836

MO0002ABBLSLDS.000. As-Built Borehole Locations and Sensor Locations for the Drift Scale Test Given in Local (DST) Coordinates. Submittal date: 02/01/2000. 147304

MO0004QGFMPICK.000. Lithostratigraphic Contacts from MO9811MWDGFM03.000 to be Qualified Under the Data Qualification Plan, TDP-NBS-GS-000001. Submittal date: 04/04/2000. 152554

MO0004RIB00035.001. Rock Thermal Expansion. Submittal date: 04/07/2000. 153848

MO0007SEPDSTPC.001. Drift Scale Test (DST) Temperature, Power, Current, and Voltage Data for November 1, 1999 through May 31, 2000. Submittal date: 07/13/2000. 153707

MO0012MWDGFM02.002. Geologic Framework Model (GFM2000). Submittal date: 12/18/2000. 153777

MO0107SEPDSTPC.003. Drift Scale Test (DST) Temperature, Power, Current, and Voltage Data for December 1, 2000 through May 31, 2001. Submittal date: 07/06/2001. 158321

MO0202SEPDSTTV.001. Drift Scale Test (DST) Temperature, Power, Current, and Voltage Data for June 1, 2001 through January 14, 2002. Submittal date: 02/28/2002. 158320

MO0301SPASIP27.004. Sampling of Stochastic Input Parameters for Rockfall Calculations and for Structural Response Calculations Under Vibratory Ground Motions. Submittal date: 01/15/2003. 161869

Table C-3. Mechanical Properties Considered for the Rock Mass in the Regional and Local Scale Calculations

Property	TCw-PTn	TSw1	TSw2-TSw3	Underlying
Young Modulus [MPa]	2540	15210	15840	15840
Poisson's ratio	0.2	0.2	0.2	0.2
Density [kg/m^3]	1613	1983	2086	1545

NOTE: These data are based on preliminary results that are similar to the information provided in Appendix E (Tables E-1 and E-16). The results from the thermal-mechanical calculation presented in this appendix are not sensitive to minor changes in mechanical properties.

The fault interfaces are calculated as cohesion-less Coulomb contacts. The friction angle is considered to be 34º (Bauer et al. 1992 [DIRS 162227]) and the stiffness (in both normal and shear directions) is computed, based on the characteristic size of the surrounding zones, so as to simulate the effect of a highly "stiff" contact. Values of 275 MN/m have been considered for the "stiff" contact based on Equation 3.4 of Theoretical Background Manual of the FLAC3D (Itasca Consulting Group 2002 [DIRS 160331]).

The thermal properties considered for the four units (TCw-PTn, TSw1, TSw2-TSw3, and underlying strata indicated in Figures C-4 and C-5) were also computed by taking averages from the detailed stratigraphic unit information (Appendix E, Section E5). The thermal properties are listed in Table C-4. The specific heat values between 95°C and 114°C are exceptionally high compared to the values of other temperature ranges (Table C-4). The high specific heat values are based on the analytical solutions presented by Nimick and Connolly (1991 [DIRS 100690]). The primary NUFT thermal calculation that is used to support the drift degradation analyses (presented in Section 6.2) does not use the high specific heat values, since consideration of latent heat effects above the boiling point is built into the NUFT code.

Table C-4. Thermal Properties Considered for the Rock Mass in the Regional and Local Scale Calculations

Property	Condition	TCw-PTn	TSw1	TSw2-TSw3	Underlying
Conductivity k	<100ºC	1.015	1.771	1.925	1.201
[W/m°C]	≥ 100ºC	0.525	1.220	1.328	0.581
Specific heat C_v	< 95ºC	1,158	939	937	1,304
[J/kg ºC]	95ºC ≤ C_v <114ºC	11,135	5,791	5,714	15,775
	≥ 114ºC	1,010	991	990	1,016
Thermal expansion α_t	<50ºC	4.46×10^{-6}	6.56×10^{-6}	7.14×10^{-6}	7.14×10^{-6}
[/ºC]	50ºC ≤ α_t <75ºC	4.46×10^{-6}	6.56×10^{-6}	7.47×10^{-6}	7.47×10^{-6}
	75ºC ≤ α_t <100ºC	4.46×10^{-6}	6.56×10^{-6}	7.46×10^{-6}	7.46×10^{-6}
	≥ 100ºC	4.46×10^{-6}	6.56×10^{-6}	9.07×10^{-6}	9.07×10^{-6}

The specific heat data used in the thermal property calculation (Table C-4) were preliminary data superseded by DTN: SN0307T0510902.003 [DIRS 164196] (Table E-19). Therefore, an impact analyses was conducted regarding the preliminary data and presented in Appendix Q2. The impact analyses indicates there are insignificant impacts on the below 95°C and over 114°C ranges, and only minor impact on the 95 to 114°C range for the local scale thermal-mechanical calculation (Section C3). An additional local scale calculation is not necessary since the local

Table E-10. Suggested Range of Mechanical Properties Developed from 11.5-in. Core Testing, Selected for Base-Case Design and Performance Analyses

Rock Mass Category	Unconfined Compressive Strength (MPa)	Estimated Young's Modulus[a] (GPa)	Cohesion[c] (MPa)			Bulk Modulus[c], K (GPa)	Shear Modulus[c], G (GPa)	Approximate Lithophysal Porosity From Laboratory Tests[b] (%)	Lithophysal Porosity Ranges for Rock Mass Categories[b] (%)
			ϕ=50	ϕ=45	ϕ=40				
1	10	1.9	1.82	2.07	2.33	1.07	0.80	35 ± 8	>25
2	15	6.4	2.73	3.11	3.50	3.54	2.65	28 ± 6	20 – 25
3	20	10.8	3.64	4.14	4.66	6.01	4.51	21 ± 4	15 – 20
4	25	15.3	4.55	5.18	5.83	8.48	6.36	13 ± 5	10 – 15
5	30	19.7	5.46	6.21	7.00	10.95	8.21	7 ± 7	<10

Source: DTNs provided in Table E-9.

[a] Young's Modulus estimated from linear fit to 11.5-in. core data given in Figure E-8.
[b] Approximated lithophysal porosity and ranges are from BSC 2004 [DIRS 172334], Table 6.4-1.
[c] Cohesion is calculated using Equation E-8. Bulk and shear modulus values are calculated based on Equations E-2 and E-3.

Table E-19. Specific Heat for Various Thermal Mechanical Units and Associated Lithostratigraphic Units

Thermal Mechanical Unit	Stratigraphic Unit	Thickness[a] (m)	Specific Heat[b] (J/kg°K)			DTN[c]
			T ≤ 95°C	95°C<T<114°C	T > 114°C	
TCw / PTn	Tpcpv3	0.0	1.2E+03	8.4E+03	1.0E+03	SN0307T0510902.003 [DIRS 164196]
	Tpcpv2	5.1	1.2E+03	8.4E+03	1.0E+03	
	Tpcpv1	2.4	1.3E+03	9.1E+03	1.0E+03	
	Tpbt4	0.5	1.3E+03	9.1E+03	1.0E+03	
	Tpy	3.8	1.3E+03	9.1E+03	1.0E+03	
	Tpbt3	3.8	1.3E+03	9.1E+03	1.0E+03	
	Tpp	5.1	1.3E+03	9.1E+03	1.0E+03	
	Tpbt2	8.3	1.3E+03	9.1E+03	1.0E+03	
	Tptrv3	1.9	1.3E+03	9.1E+03	1.0E+03	
	Tptrv2	1.2	1.3E+03	9.1E+03	1.0E+03	
	Mean (weighted by unit thickness)		*1.3E+03*	*9.0E+03*	*1.0E+03*	
TSw1	Tptrv1	1.2	8.9E+02	1.8E+03	9.9E+02	
	Tptrn	35.6	8.9E+02	2.7E+03	9.9E+02	
	Tptrl	6.1	8.9E+02	2.7E+03	9.9E+02	
	Tptpul	66.8	9.4E+02	3.6E+03	9.9E+02	
	Mean (weighted by unit thickness)		*9.2E+02*	*3.2E+03*	*9.9E+02*	
TSw2 / TSw3	Tptpmn	38.3	9.1E+02	3.0E+03	9.9E+02	
	Tptpll	95.6	9.3E+02	3.3E+03	9.9E+02	
	Tptpln	55.1	9.0E+02	2.8E+03	9.9E+02	
	Tptpv3	12.0	9.1E+02	1.7E+03	1.0E+03	
	Mean (weighted by unit thickness)		*9.1E+02*	*3.0E+03*	*9.9E+02*	
CHn1 / CHn2	Tptpv2	4.7	1.1E+03	5.1E+03	1.0E+03	
	Tptpv1	15.4	1.2E+03	6.4E+03	1.1E+03	
	Tpbt1	2.0	1.2E+03	6.4E+03	1.1E+03	
	Calico	45.5	1.4E+03	9.8E+03	1.1E+03	
	Calicobt	15.9	1.2E+03	7.6E+03	1.1E+03	
	Mean (weighted by unit thickness)		*1.3E+03*	*8.4E+03*	*1.1E+03*	

[a] Thickness of units provided in Appendix M.
[b] T = temperature.
[c] Mean values are calculated in this report and not provided by the DTNs listed in this table.

Table E-20. Thermal Expansion for Various Thermal Mechanical Units

Thermal Mechanical Unit	Thermal Expansion Coefficient (/°C)			
	25°C < T ≤ 50°C	50°C < T ≤ 75°C	75°C < T ≤ 100°C	100°C < T ≤ 125°C
TCw	7.09×10^{-6}	7.62×10^{-6}	8.08×10^{-6}	10.34×10^{-6}
PTn	4.46×10^{-6}	4.28×10^{-6}	-1.45×10^{-6}	-30.42×10^{-6}
TSw1	6.56×10^{-6}	7.32×10^{-6}	6.83×10^{-6}	6.92×10^{-6}
TSw2	7.14×10^{-6}	7.47×10^{-6}	7.46×10^{-6}	9.07×10^{-6}

T = temperature

NOTE: Source data provided by DTN: SNL01B05059301.006 [DIRS 129168]. Thermal expansion data are for saturated rock. The use of saturated data (as opposed to dry data) results in higher thermal stresses and is therefore more conservative for use in drift degradation analyses. The calculation of mean data is documented in Brodsky et al. (1997 [DIRS 100653], Table 4-4). The standard deviation data presented in Brodsky et al. (1997 [DIRS 100653], Table 4-4) are not used in this report since they are relatively small and do not significantly impact the calculation of thermal stress in this report. Additional thermal expansion data have been provided by DTN: MO0004RIB00035.001 [DIRS 153848]. The mean values for the additional data are similar to the data in this table, and the inclusion of the additional thermal expansion data would not significantly impact the results from this analysis. Therefore, the additional thermal expansion data have not been included in this report.

Q2. IMPACT ANALYSES ON SPECIFIC HEAT

The regional and local scale thermal-mechanical calculations used the weight-averaged thermal property values for the four thermal-mechanical units (Table C-4). The specific heat data used in the thermal property calculation were preliminary data superseded by DTN: SN0307T0510902.003 [DIR 164196] (Table E-19). The revised specific heat values for the thermal-mechanical units are presented in Table Q-3. Only small changes of the values occur in the below 95°C range, especially in the repository units (2 percent decrease in TSw1 and 3 percent decrease in TSw2-TSw3). The impacts of the thermal properties for the below 95°C range are estimated as minor for the FLAC3D thermal-mechanical calculation, since the value changes in the repository units (TSw1 and TSw2-TSw3) are less than 3 percent. Based on the equation-defined specific heat at constant pressure (Brodsky et al. 1997 [DIRS 100653], p. 20):

$$C_p = \frac{1}{m}\frac{\Delta Q}{\Delta T} \qquad \text{(Eq. Q-1)}$$

where m is the mass of the specimen (kg), ΔQ is the increment of heat added to the subject (J), and ΔT is the change of specimen temperature (K), the change of the temperature is also estimated to be about 3 percent.

The impact of the revised specific heat for the over 114°C range is also considered insignificant since change of the specific heat value is irrelevant (less than 0.2 percent) for the TSw2-TSw3 repository unit.

Large specific heat value changes occur in the 95°C to 114°C range (almost 50 percent decrease in the TSw2-TSw3 unit, as shown in Table Q-3). The 95°C to 114°C range is not substantial for the regional scale FLAC3D thermal-mechanical calculation, since the calculated temperatures in Appendix C were well below 95°C (Figure C-10). For the local scale calculation, the resulting temperature and thermally induced stress using the revised specific heat should be under some impact as a result of the its low specific heat value, especially for the central drift (Figure C-16). However, the rock volume for temperatures over 95°C is localized adjacent to the drift wall, and the time duration over 95°C is also limited to several hundred years. Also, the local scale thermal-mechanical calculation was only served to support and add confidence to the main thermal-mechanical calculation presented in Section 6.2. The resulting data from Section 6.2 (not from Appendix C) were used in the subsequent analyses of this document. Therefore, an additional local scale thermal-mechanical calculation is not necessary.

Table Q-3. Specific Heat Considered for the Rock Mass in the Regional and Local Scale Thermal-Mechanical Calculations (Appendix C)

Property	Condition	TCw-PTn	TSw1	TSw2-TSw3	Underlying
Preliminary specific heat C_v [J/kg ºC]	< 95ºC	1,158	939	937	1,304
	95ºC ≤ C_v <114ºC	11,135	5,791	5,714	15,775
	≥ 114ºC	1,010	991	990	1,016
Updated specific heat[a] C_v [J/kg ºC]	< 95ºC	1,300	920	910	1,300
	95ºC ≤ C_v <114ºC	9,000	3,200	3,000	8,400
	≥ 114ºC	1,000	990	990	1,100

[a] The mean values are calculated from DTN: SN0307T0510902.003 [DIRS 164196].